

Supporting Information

## Gold nanoclusters as electrocatalysts: Size, ligands, heteroatom doping, and charge dependences

Bharat Kumar,<sup>1,†,‡</sup> Tokuhisa Kawawaki,<sup>1,2,‡</sup> Nobuyuki Shimizu,<sup>1</sup> Yukari Imai,<sup>a</sup> Daiki Suzuki,<sup>a</sup> Sakiat Hossain,<sup>1</sup> Lakshmi V. Nair<sup>1</sup> and Yuichi Negishi<sup>1,2,\*</sup>

<sup>1</sup>Department of Applied Chemistry, Faculty of Science, Tokyo University of Science, 1–3 Kagurazaka, Shinjuku-ku, Tokyo 162–8601, Japan

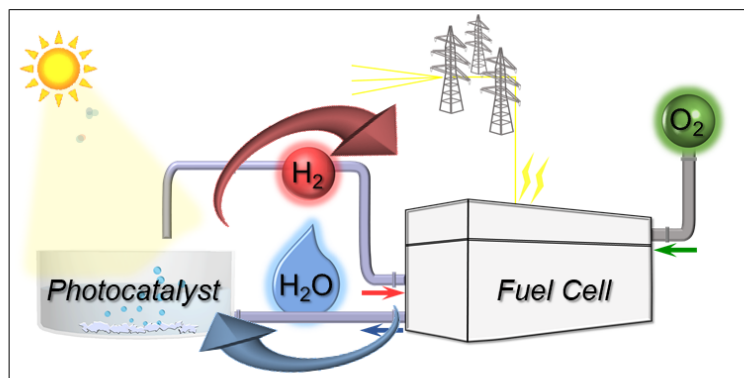
<sup>2</sup> Photocatalysis International Research Center, Tokyo University of Science, 2641 Yamazaki, Noda, Chiba 278–8510, Japan

<sup>†</sup> Present address: Department of Chemistry, M V College Buxar, Veer Kunwar Singh University, Ara, Bihar 802101, India

<sup>‡</sup> These authors contributed equally to this work.

Corresponding Author E-mail: negishi@rs.kagu.tus.ac.jp

### 1. Additional Scheme



**Scheme S1.** Expected future energy conversion system consisting of photocatalysts and fuel cell. If this system would be constructed, the fossil fuels are not consumed and the carbon dioxide is not emitted.<sup>1</sup>

## 2. Additional Table

**Table S1. Current Density of HER at Each Voltage (vs. RHE)**

Cluster	Current Density ( $\text{mA cm}^{-2} \text{ mg}^{-1}$ )					
	Actual Values <sup>a</sup>			Normalized Values <sup>b</sup>		
	-0.7 V	-0.6 V	-0.5 V	-0.7 V	-0.6 V	-0.5 V
$[\text{Au}_{25}(\text{PET})_{18}]^0$	-17.8	-10.2	-3.9	100	100	100
$[\text{Au}_{38}(\text{PET})_{24}]^0$	-16.3	-6.8	-2.2	91.3	66.8	56.8
$[\text{Au}_{130}(\text{PET})_{50}]^0$	-11.6	-4.2	-1.4	65.0	41.2	35.0
$[\text{Au}_{144}(\text{PET})_{60}]^0$	-11.3	-5.3	-2.2	63.2	52.4	56.5
$[\text{Au}_{329}(\text{PET})_{84}]^0$	-8.0	-3.8	-1.7	44.8	37.0	42.9
$[\text{Au}_{25}(\text{C6T})_{18}]^0$	-27.0	-13.9	-4.1	151.4	136.7	104.3
$[\text{Au}_{25}(\text{C12T})_{18}]^0$	-3.6	-1.2	-0.4	20.4	11.5	11.1
$[\text{Au}_{20.5}\text{Ag}_{4.5}(\text{PET})_{18}]^0$	-9.9	-4.6	-1.2	55.7	45.3	29.4
$[\text{Au}_{23.7}\text{Cu}_{1.3}(\text{PET})_{18}]^0$	-3.2	-0.6	-0.1	18.0	5.6	2.4
$[\text{Au}_{24}\text{Pd}(\text{PET})_{18}]^0$	-27.1	-12.1	-5.4	151.7	119.2	137.6
$[\text{Au}_{25}(\text{PET})_{18}]^-$	-26.0	-13.9	-8.1	145.7	136.7	206.0

<sup>a</sup> These values were estimated from Figure 1(a), Figure 3(a) and Figure 5(a). <sup>b</sup> These values are normalized with that of  $[\text{Au}_{25}(\text{PET})_{18}]^0$ .

**Table S2. Current Density of OER at Each Voltage (vs. RHE)**

Cluster	Current Density ( $\text{mA cm}^{-2} \text{ mg}^{-1}$ )					
	Actual Values <sup>a</sup>			Normalized Values <sup>b</sup>		
	2.2 V	2.1 V	2.0 V	2.2 V	2.1 V	2.0 V
$[\text{Au}_{25}(\text{PET})_{18}]^0$	8.55	3.99	1.68	100	100	100
$[\text{Au}_{38}(\text{PET})_{24}]^0$	5.63	2.58	1.29	65.9	64.7	76.9
$[\text{Au}_{130}(\text{PET})_{50}]^0$	4.52	1.97	0.87	52.9	49.4	51.8
$[\text{Au}_{144}(\text{PET})_{60}]^0$	3.56	1.57	0.70	41.6	39.3	41.6
$[\text{Au}_{329}(\text{PET})_{84}]^0$	3.19	1.55	0.80	37.3	38.8	47.7
$[\text{Au}_{25}(\text{C6T})_{18}]^0$	8.95	3.99	1.87	104.7	103.2	111.1
$[\text{Au}_{25}(\text{C12T})_{18}]^0$	1.23	0.58	0.43	14.4	14.5	25.8
$[\text{Au}_{20.5}\text{Ag}_{4.5}(\text{PET})_{18}]^0$	7.39	3.49	1.42	86.5	87.6	84.8
$[\text{Au}_{23.7}\text{Cu}_{1.3}(\text{PET})_{18}]^0$	8.65	3.75	1.57	101.2	94.1	93.4
$[\text{Au}_{24}\text{Pd}(\text{PET})_{18}]^0$	9.47	3.92	1.51	110.8	98.2	89.7
$[\text{Au}_{25}(\text{PET})_{18}]^-$	10.31	4.83	2.75	120.6	121.2	164.0

<sup>a</sup> These values were estimated from Figure 1(c), Figure 3(c) and Figure 5(c). <sup>b</sup> These values are normalized with that of  $[\text{Au}_{25}(\text{PET})_{18}]^0$ .

**Table S3. Current Density of ORR at Each Voltage (vs. RHE)**

Cluster	Current Density ( $\text{mA cm}^{-2} \text{ mg}^{-1}$ )					
	Actual Values <sup>a</sup>			Normalized Values <sup>b</sup>		
	-0.2 V	-0.1 V	-0 V	-0.2 V	-0.1 V	-0 V
$[\text{Au}_{25}(\text{PET})_{18}]^0$	-0.85	-0.87	-0.75	100	100	100
$[\text{Au}_{38}(\text{PET})_{24}]^0$	-0.49	-0.40	-0.33	57.0	46.2	44.0
$[\text{Au}_{130}(\text{PET})_{50}]^0$	-0.44	-0.33	-0.18	51.2	38.4	24.6
$[\text{Au}_{144}(\text{PET})_{60}]^0$	-0.30	-0.23	-0.14	35.3	26.2	19.2
$[\text{Au}_{329}(\text{PET})_{84}]^0$	-0.14	-0.05	-0.03	16.8	5.9	4.7
$[\text{Au}_{25}(\text{C6T})_{18}]^0$	-0.91	-1.05	-0.67	106.8	121.3	89.3
$[\text{Au}_{25}(\text{C12T})_{18}]^0$	-0.54	-0.40	-0.26	63.7	46.5	34.2
$[\text{Au}_{20.5}\text{Ag}_{4.5}(\text{PET})_{18}]^0$	-0.78	-1.04	-0.72	91.4	119.9	96.2
$[\text{Au}_{23.7}\text{Cu}_{1.3}(\text{PET})_{18}]^0$	-0.75	-0.81	-0.62	88.4	93.0	82.4
$[\text{Au}_{24}\text{Pd}(\text{PET})_{18}]^0$	-0.95	-0.91	-0.78	111.8	104.5	104.2
$[\text{Au}_{25}(\text{PET})_{18}]^-$	-1.13	-0.72	-0.41	133.4	83.2	54.2

<sup>a</sup> These values were estimated from Figure 1(e), Figure 3(e) and Figure 5(e). <sup>b</sup> These values are normalized with that of  $[\text{Au}_{25}(\text{PET})_{18}]^0$ .

### 3. Additional Figures

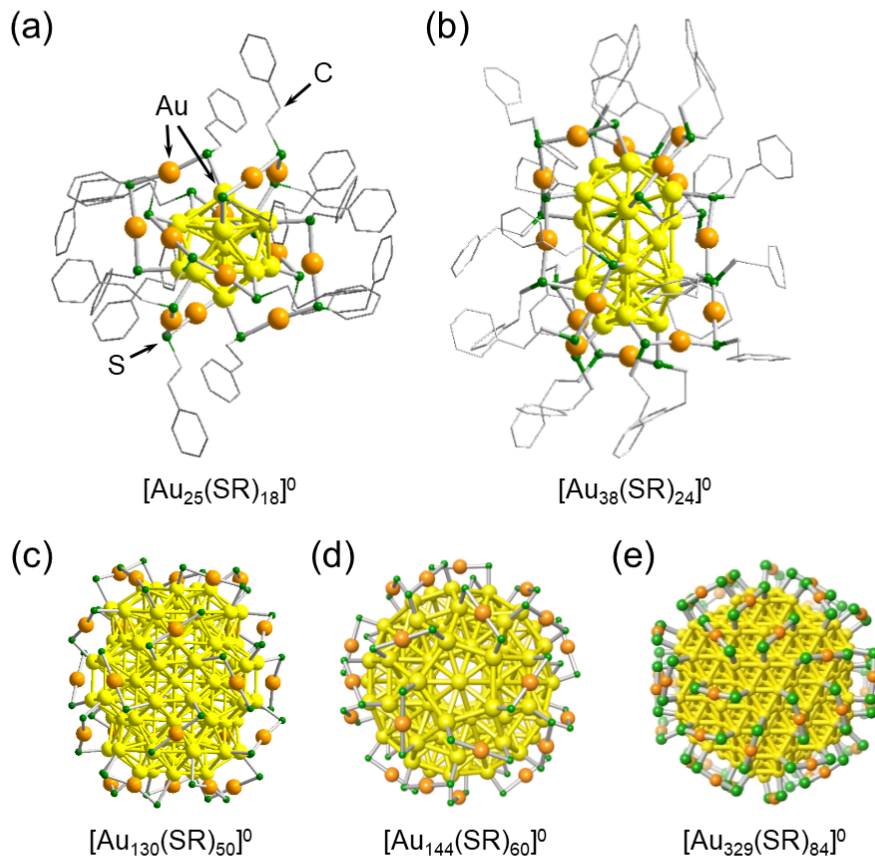


**Figure S1.** Geometrical structures of (a)  $[\text{Au}_{25}(\text{SR})_{18}]^0$ ,<sup>2</sup> (b)  $[\text{Au}_{38}(\text{SR})_{24}]^0$ ,<sup>3</sup> (c)  $[\text{Au}_{130}(\text{SR})_{50}]^0$ ,<sup>4</sup> (d)  $[\text{Au}_{144}(\text{SR})_{60}]^0$ ,<sup>5</sup> and (e)  $[\text{Au}_{329}(\text{SR})_{84}]^0$  ( $\text{SR} = 2\text{-phenylethanethiolate (PET)} \text{ or } 4\text{-methylbenzenethiolate}$ ).<sup>6</sup> The geometrical structures of (a)–(d) were determined by single crystal X-ray structural diffraction (SCXRD), whereas the geometrical structure of (e) is the proposed structure on the basis of the chemical composition.<sup>6</sup>

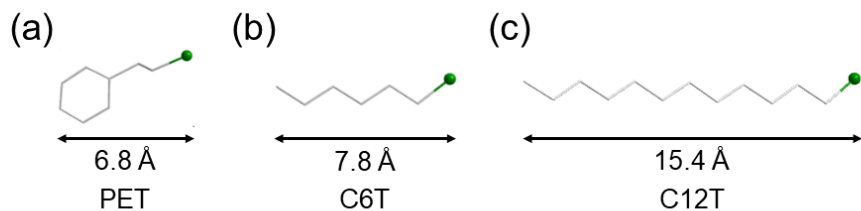


**Figure S2.** Geometrical structures of (a) PET, (b) 1-hexanethiolate (C6T), (c) 1-dodecanethiolate (C12T). The length of ligand was estimated from the geometrical structures.<sup>2,7,8</sup>

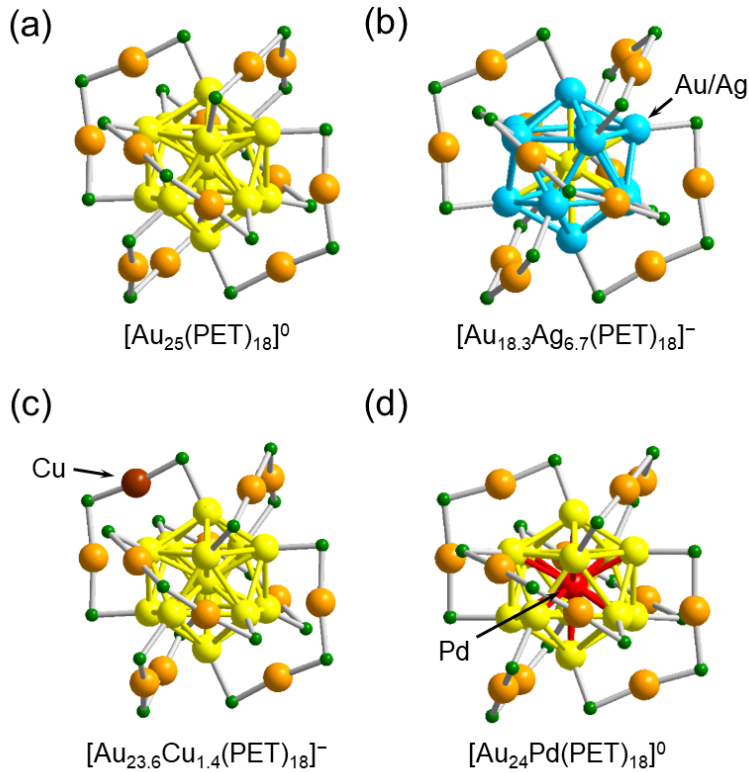


**Figure S3.** Geometrical structures of (a)  $\text{Au}_{25}(\text{PET})_{18}$ ,<sup>2</sup> (b)  $\text{Au}_{18.3}\text{Ag}_{6.7}(\text{PET})_{18}$ ,<sup>9</sup> (c)  $\text{Au}_{23.6}\text{Cu}_{1.4}(\text{PET})_{18}$ ,<sup>10</sup> and (d)  $\text{Au}_{24}\text{Pd}(\text{PET})_{18}$ .<sup>11</sup> The geometrical structures of (a) and (b) were determined by SCXRD for their anion forms. However, since  $[\text{Au}_{25}(\text{PET})_{18}]^-$  and  $[\text{Au}_{25}(\text{PET})_{18}]^0$  have similar framework structures,<sup>2</sup>  $[\text{Au}_{24.6}\text{Ag}_{0.4}(\text{PET})_{18}]^0$  is also considered to have a similar geometrical structure to that of the anion form (b). The geometrical structure of (d) is determined by SCXRD for the neutral form ( $[\text{Au}_{24}\text{Pd}(\text{PET})_{18}]^0$ ). The geometrical structure of (c) is the proposed structure on the basis of the result obtained by extended X-ray absorption fine structure analysis.<sup>10</sup>

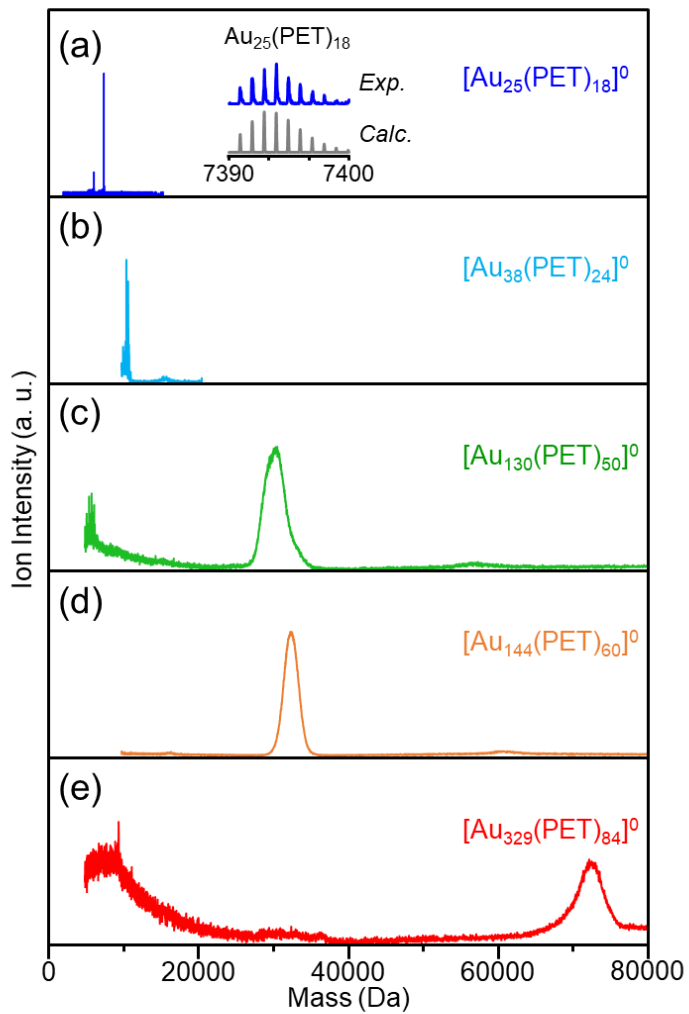


**Figure S4.** MALDI mass spectra of (a)  $[\text{Au}_{25}(\text{PET})_{18}]^0$ , (b)  $[\text{Au}_{38}(\text{PET})_{24}]^0$ , (c)  $[\text{Au}_{130}(\text{PET})_{50}]^0$ , (d)  $[\text{Au}_{144}(\text{PET})_{60}]^0$  and (e)  $[\text{Au}_{329}(\text{PET})_{84}]^0$ . These mass spectra include or consists of the laser-fragments of the parent clusters. These mass spectra include only the peaks due to the parent clusters.<sup>12</sup>

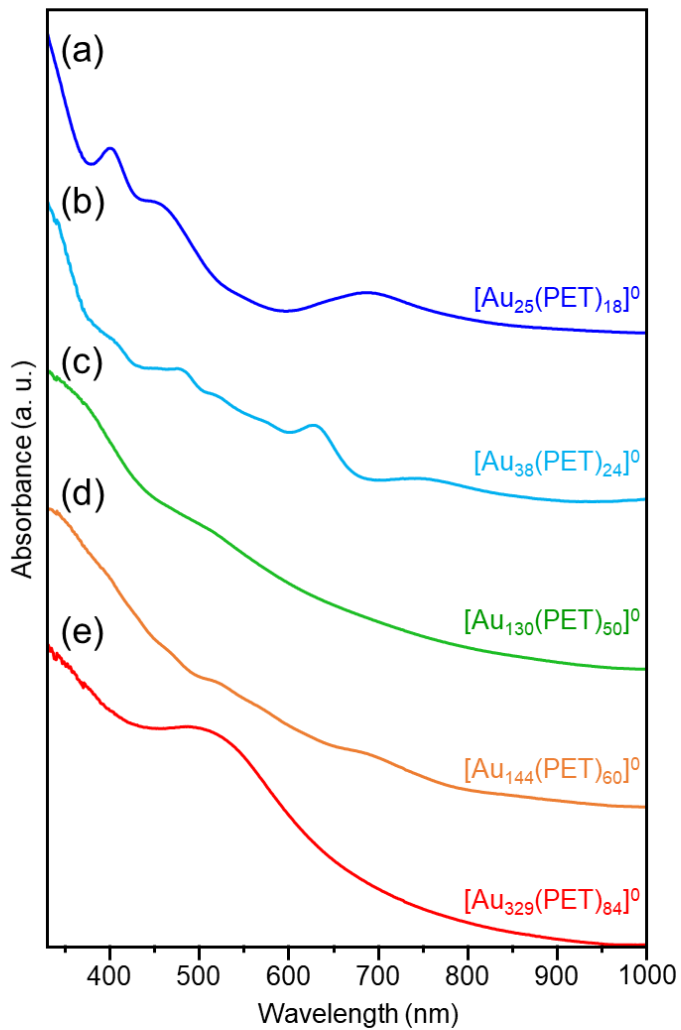


**Figure S5.** Optical absorption spectra of (a)  $[\text{Au}_{25}(\text{PET})_{18}]^0$ , (b)  $[\text{Au}_{38}(\text{PET})_{24}]^0$ , (c)  $[\text{Au}_{130}(\text{PET})_{50}]^0$ , (d)  $[\text{Au}_{144}(\text{PET})_{60}]^0$  and (e)  $[\text{Au}_{329}(\text{PET})_{84}]^0$ . These spectra are well consistent with the reported spectra for these clusters,<sup>2,5,13–15</sup> indicating that the synthesized clusters have high purity.

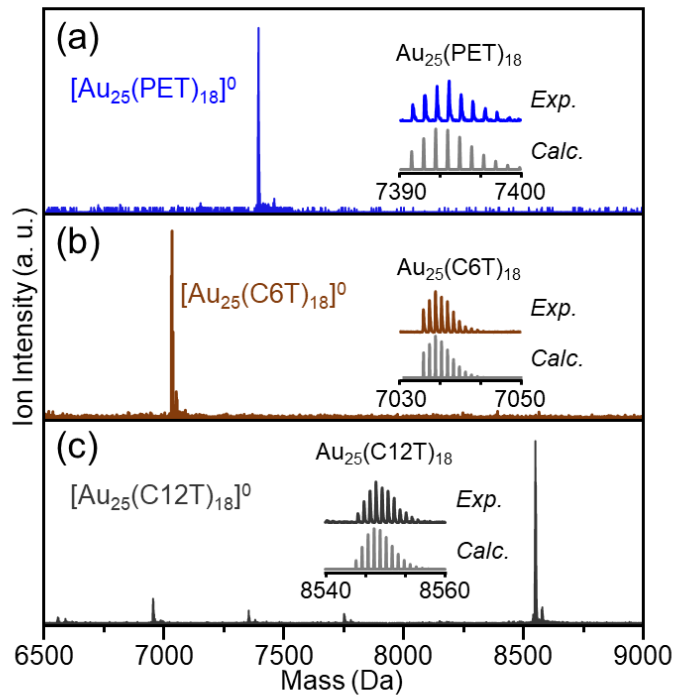


**Figure S6.** MALDI mass spectra of (a)  $[\text{Au}_{25}(\text{PET})_{18}]^0$ , (b)  $[\text{Au}_{25}(\text{C}_6\text{T})_{18}]^0$ , and (c)  $[\text{Au}_{25}(\text{C}_{12}\text{T})_{18}]^0$ .

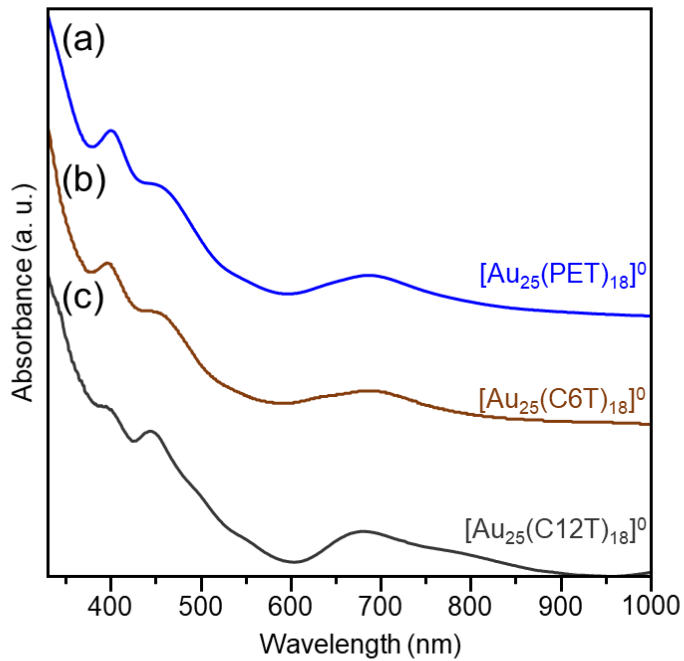


**Figure S7.** Optical absorption spectra of (a)  $[\text{Au}_{25}(\text{PET})_{18}]^0$ , (b)  $[\text{Au}_{25}(\text{C}_6\text{T})_{18}]^0$ , and (c)  $[\text{Au}_{25}(\text{C}_{12}\text{T})_{18}]^0$ . These spectra are well consistent with the literature,<sup>2,16</sup> indicating that the synthesized clusters have high purity.

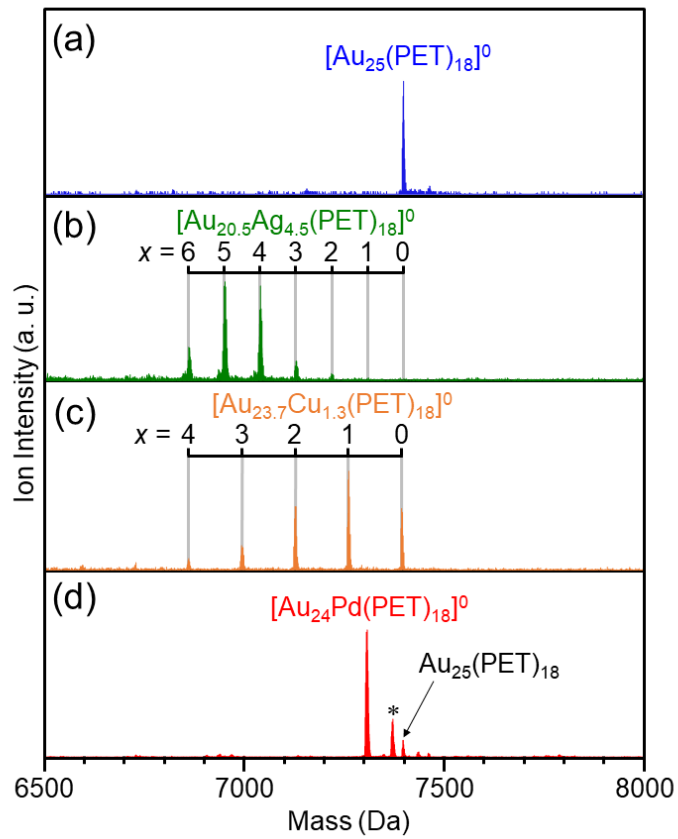


**Figure S8.** MALDI mass spectra of (a)  $[\text{Au}_{25}(\text{PET})_{18}]^0$ , (b)  $[\text{Au}_{20.5}\text{Ag}_{4.5}(\text{PET})_{18}]^0$ , (c)  $[\text{Au}_{23.7}\text{Cu}_{1.3}(\text{PET})_{18}]^0$ , and (d)  $[\text{Au}_{24}\text{Pd}(\text{PET})_{18}]^0$ . The asterisk (\*) indicates  $[\text{Au}_{24}\text{Pd}(\text{PET})_{17}(\text{C12T})]^0$ .

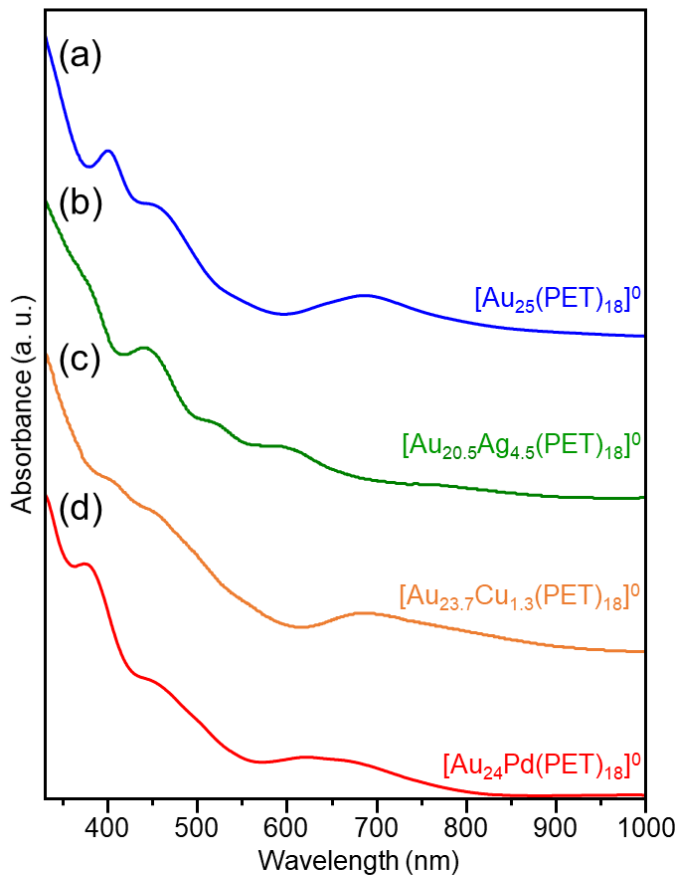


**Figure S9.** Optical absorption spectra of (a)  $[\text{Au}_{25}(\text{PET})_{18}]^0$ , (b)  $[\text{Au}_{20.5}\text{Ag}_{4.5}(\text{PET})_{18}]^0$ , (c)  $[\text{Au}_{23.7}\text{Cu}_{1.3}(\text{PET})_{18}]^0$ , and (d)  $[\text{Au}_{24}\text{Pd}(\text{PET})_{18}]^0$ . These spectra are well consistent with the reported spectra for these clusters.<sup>2,17-19</sup>

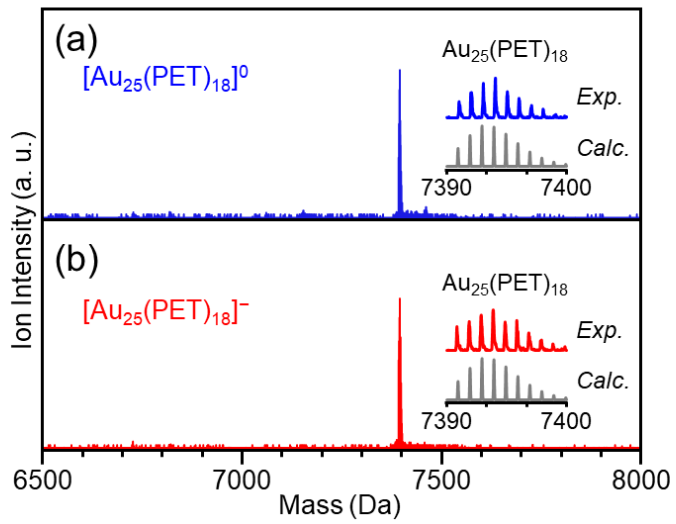


**Figure S10.** MALDI mass spectra of (a)  $[\text{Au}_{25}(\text{PET})_{18}]^0$  and (b)  $[\text{Au}_{25}(\text{PET})_{18}]^-$ .

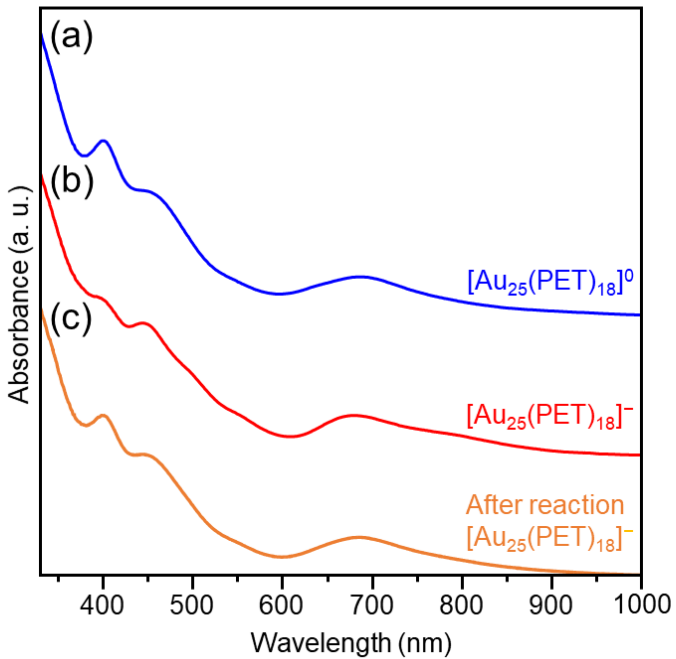


**Figure S11.** Optical absorption spectra of (a)  $[\text{Au}_{25}(\text{PET})_{18}]^0$  and (b)  $[\text{Au}_{25}(\text{PET})_{18}]^-$ . These spectra are well consistent with the reported spectra for those clusters,<sup>2</sup> indicating that the synthesized clusters have high purity. The spectra (c) shows the optical absorption spectra of  $[\text{Au}_{25}(\text{PET})_{18}]^-$  after the electrochemical measurement. This spectral feature is quite similar to that of  $[\text{Au}_{25}(\text{PET})_{18}]^0$ , indicating that  $[\text{Au}_{25}(\text{PET})_{18}]^-$  was oxidized to  $[\text{Au}_{25}(\text{PET})_{18}]^0$  during the electrochemical measurement.

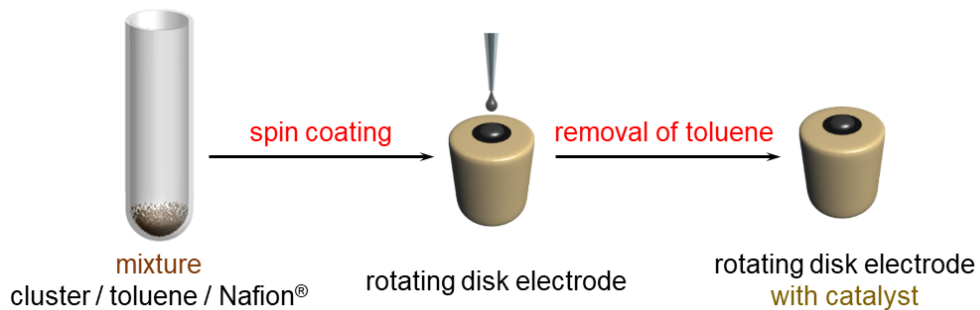


**Figure S12.** Schematic diagram for the preparation of working electrode with catalysts.

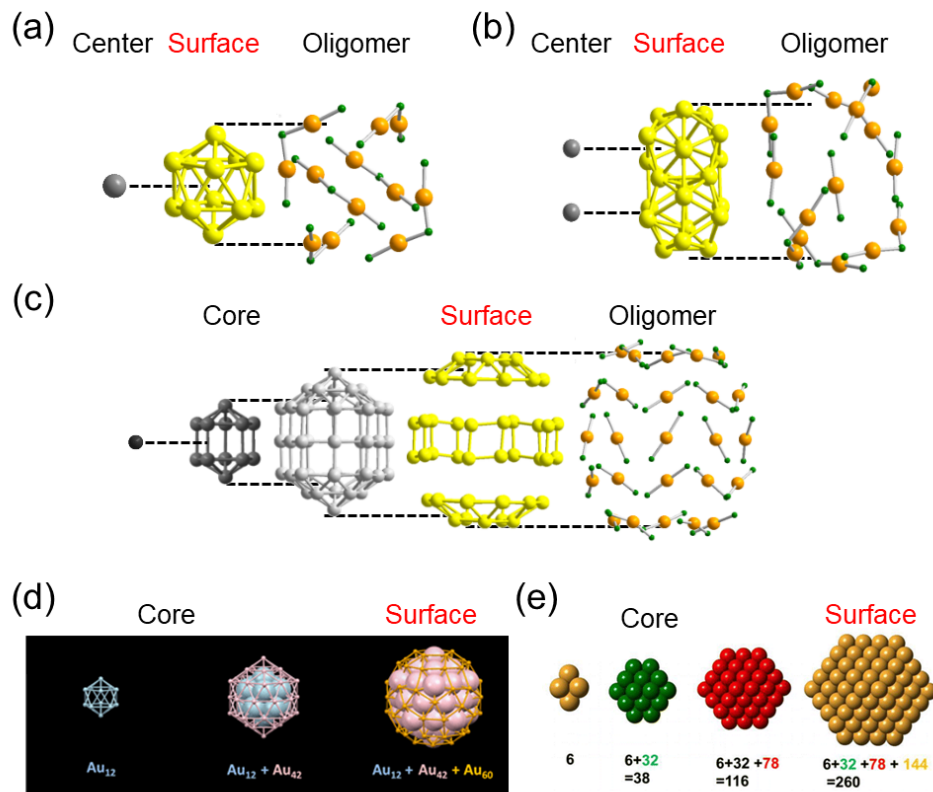


**Figure S13.** Surface atoms used for the estimation of the number of surface atoms in each sample (Table 1); (a) [Au<sub>25</sub>(PET)<sub>18</sub>]<sup>0,2</sup> (b) [Au<sub>38</sub>(PET)<sub>24</sub>]<sup>0,3</sup> (c) [Au<sub>130</sub>(PET)<sub>50</sub>]<sup>0,4</sup> (d) [Au<sub>144</sub>(PET)<sub>60</sub>]<sup>0,20</sup> and (e) [Au<sub>329</sub>(PET)<sub>84</sub>]<sup>0,6</sup>. Reprinted with permission from refs 5 and 6. Copyright 2015 American Chemical Society.

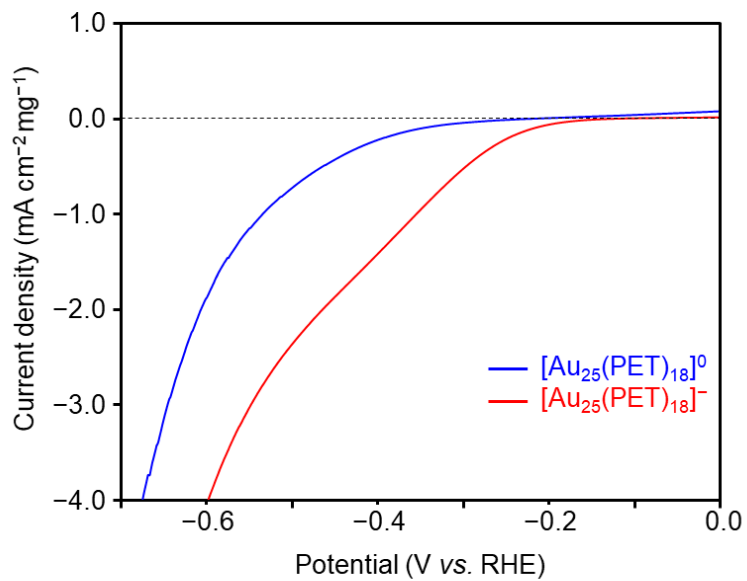


**Figure S14.** Comparison of HER activity between  $[\text{Au}_{25}(\text{PET})_{18}]^0$  and  $[\text{Au}_{25}(\text{PET})_{18}]^-$ . This result indicates that  $[\text{Au}_{25}(\text{PET})_{18}]^-$  shows higher activity than  $[\text{Au}_{25}(\text{PET})_{18}]^0$ . However, as shown in Figure S11(b)(c),  $[\text{Au}_{25}(\text{PET})_{18}]^-$  is oxidized to  $[\text{Au}_{25}(\text{PET})_{18}]^0$  during the electrochemical measurement, indicating that  $[\text{Au}_{25}(\text{PET})_{18}]^-$  is not stable under the electrochemical measurement condition.

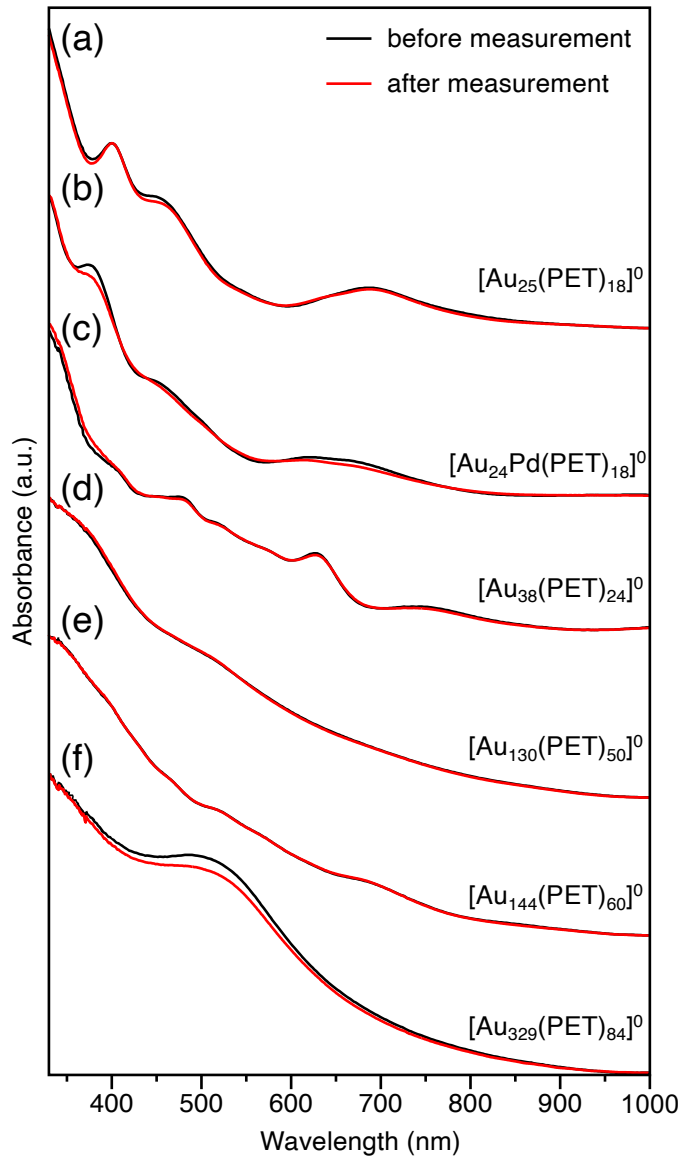


**Figure S15.** Comparison of optical absorption spectra before and after the electrochemical measurements; (a)  $[\text{Au}_{25}(\text{PET})_{18}]^0$ , (b)  $[\text{Au}_{24}\text{Pd}(\text{PET})_{18}]^0$ , (c)  $[\text{Au}_{38}(\text{PET})_{24}]^0$ , (d)  $[\text{Au}_{130}(\text{PET})_{50}]^0$ , (e)  $[\text{Au}_{144}(\text{PET})_{60}]^0$ , and (f)  $[\text{Au}_{329}(\text{PET})_{84}]^0$ .

#### 4. References

1. Z. W. Seh, J. Kibsgaard, C. F. Dickens, I. Chorkendorff, J. K. Nørskov and T. F. Jaramillo, *Science*, 2017, **355**, eaad4998.
2. M. Zhu, W. T. Eckenhoff, T. Pintauer and R. Jin, *J. Phys. Chem. C*, 2008, **112**, 14221–14224.
3. H. Qian, W. T. Eckenhoff, Y. Zhu, T. Pintauer and R. Jin, *J. Am. Chem. Soc.*, 2010, **132**, 8280–8281.
4. Y. Chen, C. Zeng, C. Liu, K. Kirschbaum, C. Gayathri, R. R. Gil, N. L. Rosi and R. Jin, *J. Am. Chem. Soc.*, 2015, **137**, 10076–10079.
5. N. Yan, N. Xia, L. Liao, M. Zhu, F. Jin, R. Jin and Z. Wu, *Sci. Adv.*, 2018, **4**, eaat7259.
6. C. Kumara, X. Zuo, J. Ilavsky, D. Cullen and A. Dass, *J. Phys. Chem. C*, 2015, **119**, 11260–11266.
7. D. K. Tarakci, S. Berber, Y. Zorlu, D. Atilla, V. Ahsen and F. Dumoulin, *New J. Chem.*, 2015, **39**, 3929–3935.
8. Z. Yang, A. B. Smetana, C. M. Sorensen and K. J. Klabunde, *Inorg. Chem.*, 2007, **46**, 2427–2431.
9. C. Kumara, C. M. Aikens and A. Dass, *J. Phys. Chem. Lett.*, 2014, **5**, 461–466.
10. S. Yamazoe, W. Kurashige, K. Nobusada, Y. Negishi and T. Tsukuda, *J. Phys. Chem. C*, 2014, **118**, 25284–25290.
11. S. Tian, L. Liao, J. Yuan, C. Yao, J. Chen, J. Yang and Z. Wu, *Chem. Commun.*, 2016, **52**, 9873–9876.
12. Y. Negishi, T. Nakazaki, S. Malola, S. Takano, Y. Niihori, W. Kurashige, S. Yamazoe, T. Tsukuda and H. Häkkinen, *J. Am. Chem. Soc.*, 2015, **137**, 1206–1212.
13. C. Zeng, C. Liu, Y. Pei and R. Jin, *ACS Nano*, 2013, **7**, 6138–6145.
14. V. R. Jupally and A. Dass, *Phys. Chem. Chem. Phys.*, 2014, **16**, 10473–10479.
15. C. Kumara and A. Dass, *Anal. Chem.*, 2014, **86**, 4227–4232.
16. Y. Lu, Y. Jiang, X. Gao and W. Chen, *Chem. Commun.*, 2014, **50**, 8464–8467.
17. Y. Negishi, T. Iwai and M. Ide, *Chem. Commun.*, 2010, **46**, 4713–4715.
18. E. Gottlieb, H. Qian and R. Jin, *Chem.-Eur. J.*, 2013, **19**, 4238–4243.
19. H. Qian, E. Barry, Y. Zhu and R. Jin, *Acta Phys. -Chim. Sin.*, 2011, **27**, 513–519.
20. X. Kang and M. Zhu, *Coord. Chem. Rev.*, 2019, **394**, 1–38.